UCID- 20371

VULTURE MANUAL

Miles L. Loyd

February 25, 1985

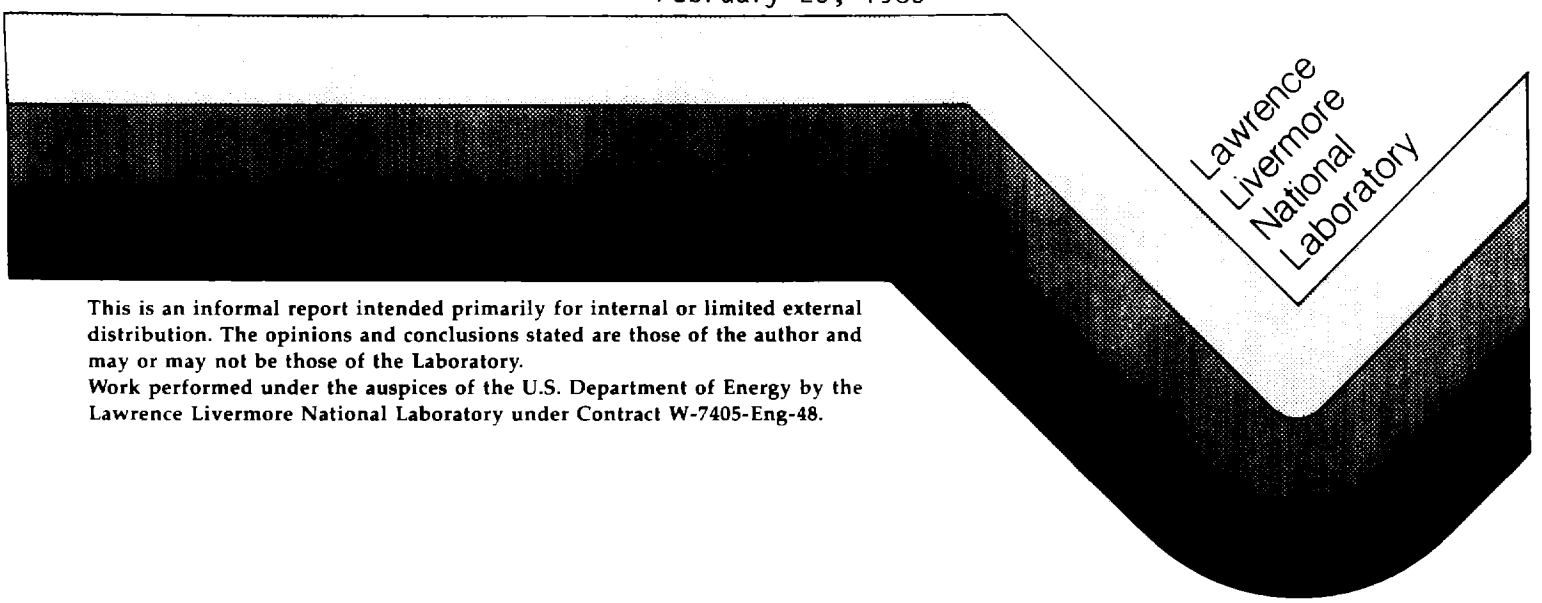

Work performed under the auspices of the U.S. Department of Energy by the Lawrence Livermore National Laboratory under Contract W-7405-Eng-48.

Printed in the United States of Ameri
Available from
National Technical Information Servi
U.S. Department of Commerce
5285 Port Royal Road
Springfield, VA 22161
Price: Printed Copy $ Microfiche $3.50

Page Range	Domestic Price	Page Range	Domestic Price
001-025	$ 7.00	326-350	$ 26.50
026-050	8.50	351-375	28.00
051-075	10.00	376-400	29.50
076-100	11.50	401-426	31.00
101-125	13.00	427-450	32.50
126-150	14.50	451-475	34.00
151-175	16.00	476-500	35.50
176-200	17.50	501-525	37.00
201-225	19.00	526-550	38.50
226-250	20.50	551-575	40.00
251-275	22.00	576-600	41.50
276-300	23.50	601-up[1]	
301-325	25.00		

[1]Add 1.50 for each additional 25 page increment, or portion thereof from 601 pages up.

VULTURE MANUAL

February 12, 1985

M. L. Loyd
University of California
Lawrence Livermore National Laboratory
Livermore, California 94550

TABLE OF CONTENTS

1. CODE DESCRIPTION

1.1. OVERVIEW

This part of the VULTURE Manual describes the VULTURE code and its operation. Part two discusses code validation to date.

VULTURE is a one dimensional electrostatic particle and field code to simulate electron beam devices such as klystrons or virtual cathode oscillators. It uses particle and cell calculation methods.[1-4] VULTURE includes the relativistic motion of electrons and the nonrelativistic motion of protons and ions. The one dimensional model may be thought of as particle sheets parallel to the y-z plane moving in the x direction. Electric field, charge density and potential are calculated as a function of x. No magnetic fields are included and the plasma is collisionless.

The model is bounded by end plates at x=0 and at a maximum value of x. These end plates are referred to as grids. Additional grids may be located within these bounds, and external circuits connected between the grids provide for the simulation of microwave cavities. Electrical energy is extracted by resistive loss in these circuits.

In addition to initial electron, proton and ion conditions, electrons can be emitted and absorbed by all grids including the model boundaries. This electron emission can be varied in both spectrum and time for each grid.

VULTURE is run on the CDC 7600 computers. Typical problems require a few minutes of computer time. Very small problems can run in well under one minute, and very large problems with ~ 50,000 particles and tens of thousands of time steps may require hundreds of minutes. The source code is written in

LLLTRAN for the CHAT complier, and it uses library routines on the LLNL main computer system.

1.2. DESCRIPTION

This section describes each of the major features modeled in VULTURE. The general structure of the VULTURE model is shown in Fig. 1. The units used are SI, except that temperatures are expressed in electron-volts. In this 1-D model, most parameters such as charge, momentum, and current are based on unit area. Thus, calculations represent coulombs per square meter of particle sheet, etc.

1.2.1. Cells

As shown in Fig. 1, the x axis is divided into NZ cells. Each cell has a width DX. The boundaries of the system are the centers of cells 1 and NZ, at x = 0 and at XMAX. Any intermediate cell, IZ, is located by its center. In addition to using the concept of the cell, a zone, IZ, is defined extending from the center of the IZ cell to the center of the IZ+1 cell.

In the particle and cell calculation routines, the charges of the particles in the neighborhood of each cell are summed by using a linear position function to assign a portion of each particle charge to the cell. The cell charge, QZ(IZ), resulting from this summation is located at the center of the cell as illustrated in Fig. 1. Using these cell charges, the electric fields, E(IZ), at the boundaries of the cell are calculated. Subsequent particle motion is calculated based on these fields. The cycle is then repeated for the next time interval, DT.

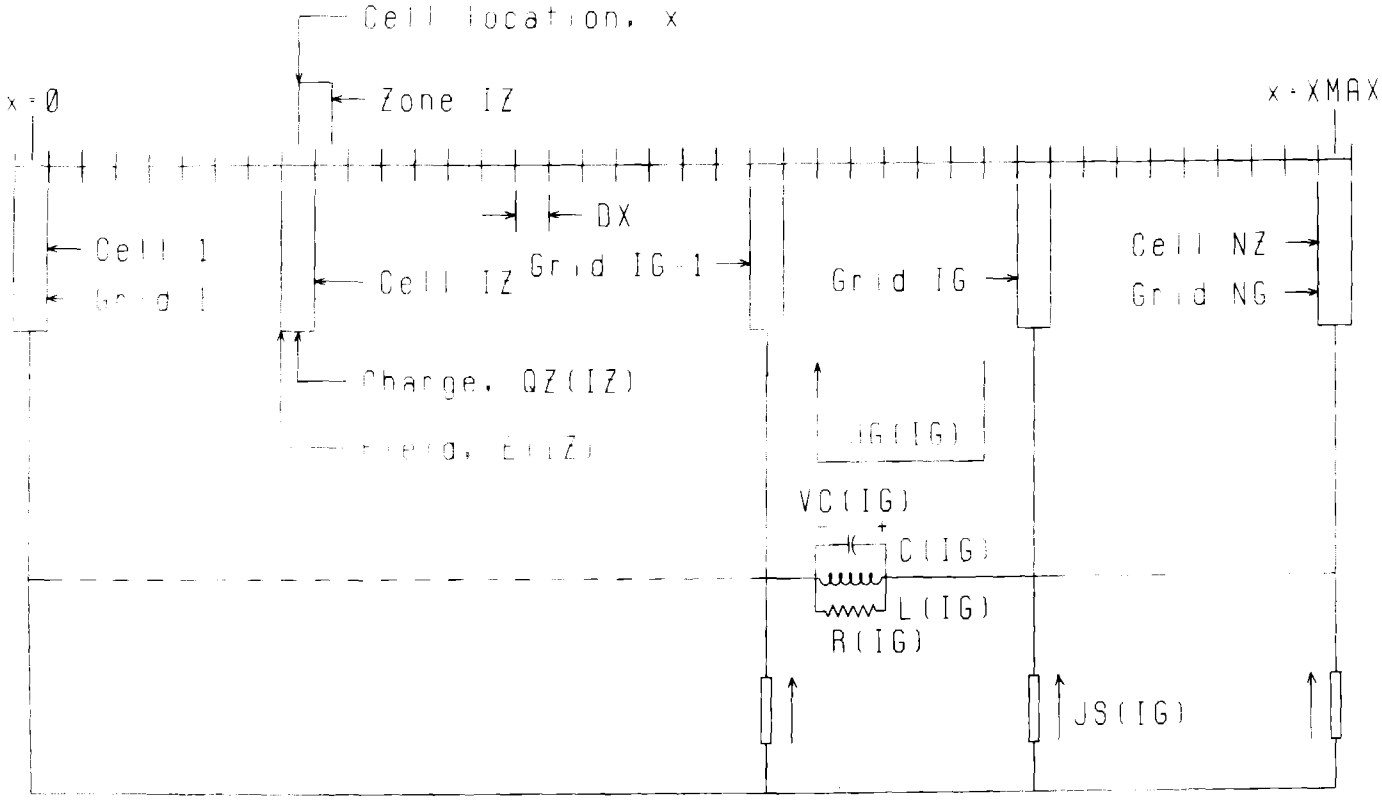
Cell location, x
x = 0
Zone IZ
x = XMAX
DX
Cell 1
Grid 1
Cell IZ
Grid IG-1
Grid IG
Cell NZ
Grid NG
Charge, QZ(IZ)
Field, EF(IZ)
JG(IG)
VC(IG)
C(IG)
L(IG)
R(IG)
JS(IG)

Figure 1

1.2.2. Grids

The ends of the system at cells 1 and NZ constitute grids or end plates with particular properties. These always exist as the system boundaries. In calculations, electrons exiting past the centers of these two grids are totally absorbed. Ions or protons passing the centers of these two grids are totally reflected so they remain in the system. (An option to absorb the protons and ions at one grid and make them available at another may be added in the future.)

Additional grids may be defined at any of the cells. For each of these additional grids, a transparency, which can have any value from 0 to 1, is defined as input data. An electron particle passing through a grid is partially absorbed, and both its charge and momentum are reduced depending on the transparency. In addition to absorbing electrons, all grids can emit energetic electrons. This emission is described below.

Electrons that are emitted or absorbed by the grid are coupled to external electric circuits as indicated in Fig. 1. In the field calculations, the potential between two successive grids is matched to the circuit voltage by assigning a grid current, JG(IG), that flows from the grid to the circuit. In addition to accounting for the electron emission and absorption, this current provides for the dD/dt displacement current in the intergrid space.

1.2.3. Protons, Ions, and Initial Electrons

In the initialization of a problem, protons and ions may be uniformly distributed throughout the space of the system, and excess numbers of protons maybe located at the grids. When this option is used the charge of the protons and ions is automatically neutralized by the addition of equal numbers of electrons. These protons, ions and electrons are introduced to the system with separate Maxwellian energy distributions.

Input data, for spacially distributed particles, specifies the space number density of ions and protons, the particle temperature, and the number of macroparticles to represent these ions and protons. The macroparticles are distributed evenly in space between x=0 and XMAX. Particles are not located precisely at x=0 or XMAX. They are offset very slightly inside the device. The space charge neutralization electrons are added at the same locations as the ions and protons. This scheme is used to avoid the immediate absorption of the electrons at the end grids of the system.

Input data for grid protons includes the number of macroparticles to be used and the area density of protons to be available at each grid. The number of macroparticles at each grid is automatically adjusted so the particles represent approximately equal numbers of protons. The grid protons are initialized at the same temperature as space protons.

1.2.4. Electron Emission

Electron beams may be emitted from any of the grids including the end plates. These electrons are assigned both energy levels and temperatures, so the temperature is an energy distribution about the mean beam energy. As the

temperature approaches zero, the beam becomes more nearly monoenergetic at the assigned energy. When the assigned temperature is high and the energy is low, the beam has a Maxwellian energy distribution. The procedure for assigning the energy to the macroparticle is to calculate the momentum resulting from the beam energy and the momentum resulting from the mean energy for the temperature distribution. The momentum due to temperature is multiplied by a random number that results in a Gaussian momentum distribution for the set of particles. This temperature component is then added to the momentum component due to the beam energy. This sum of the two momentum components is assigned as the momentum of the particle. Thus, the assigned beam energy and temperature are used to determine initial to particle momentum for further code calculations.

The current density of each electron beam is assigned as input data. This current density is used to determine the particle charge at the same time the initial momentum is determined. However, there are two additional controls of the beam current that influence the assigned particle charge. One is the number of particles created in each time step, and the other is the flux function. The current density that is assigned as input data is multiplied by a flux function that provides for scaling the emission. This flux function also provides for time variation of the emission of the beam. Multiple beams may be emitted from each grid. This combined with the flux function for each beam provides for time variation of the emission spectrum. The different beams emitted from a grid may have different energies, temperatures, and flux functions.

A flux function is defined for each energy level. Each flux function is a piece-wise linear function as illustrated in Fig. 2. One set of break-point times is used for all flux functions. The amplitude of each flux function at each break-point time is specified in the input data. The first point in the flux function is always at zero amplitude at zero time. However, the second point may be less than DT to give the effect of a step function input. The last break point time should exceed the problem run time to avoid ambiguity. The flux function need not return to zero if the last break point time exceeds the problem run time. In addition to the time dependent flux, a flux amplitude scaling input called FLUXAMP is used. All flux functions are scaled by FLUXAMP to determine the actual particle emission. Consequently, for each grid and for each energy level a particle is emitted that has a momentum and a charge that is determined by the input energy and current density as well as the flux function and flux amplitude. The individual particle momentum and charge is based on the current density resulting from the product of the input current density, the time varying flux function, and the flux scaling function.

1.2.5. Circuits

As shown in Fig. 1 the circuits connected to the grids are simple parallel RLC circuits with additional current sources, JS(IG). The parallel RLC circuit is modeled as occurring between two adjacent grids. This is somewhat similar to the fundamental cavity configuration in a beam device such as a klystron. A circuit of this type is between each pair of adjacent grids. Grid 1 is considered the ground or reference potential for circuit

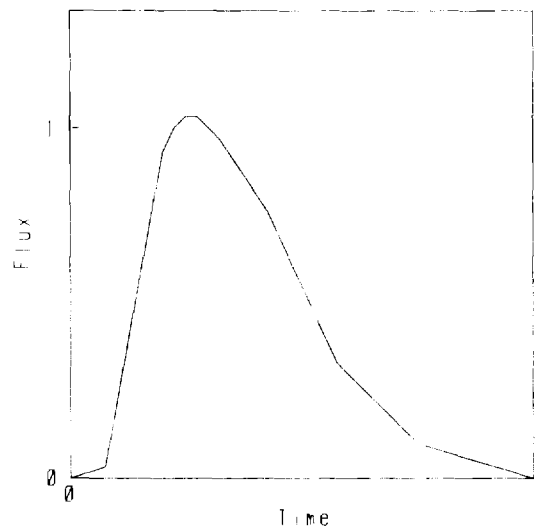

Figure 2

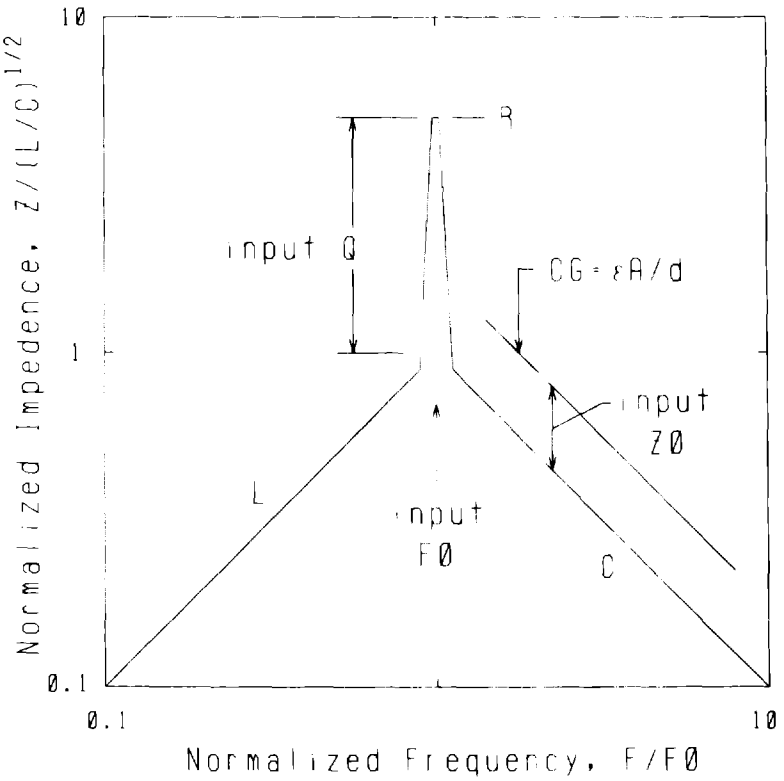

Figure 3

calculations, and the current sources are modeled as injecting currents into the circuits from Grid 1. In addition, the grid current, JG(IG), that couples the circuit equations to the field equations is injected through the circuit between the two adjacent grids.

The impedance characteristics of a circuit of this type are illustrated in Fig. 3. The impedance of an inductor, L, is proportional to frequency. The impedance of a capacitor, C, is inversely proportional to frequency. The intergrid capacitance, $\varepsilon A/d$, is the minimum capacitance that can exist within the system. That is the physical capacitance that would occur between the two adjacent grids. The circuit capacitance will normally be somewhat greater, resulting in a lower impedance as illustrated in Fig. 3. As input data, the ratio, $\varepsilon A/dC$, of these two capacitances is input as the variable ZO. The maximum value of ZO should be 0.7. The resonant frequency, FO, in Hertz is input. This combination of frequency and impedance determines the inductance and capacitance that are actually attributed to the equivalent circuit. As input data, the circuit Q, which is equal to the ratio $R/(L/C)^{1/2}$, is specified. This value of Q in combination with the resonant frequency and the impedance will be converted to the value of R for circuit calculations. In setting up a problem ZO, FO, and Q are input data.

1.2.6. Input Data

Fig. 4 is a sample input data file with annotation. All data fields have been filled with numbers and signs whether required or not.

Lines 1 through 24 contain the input data. Lines 28 through 55 provide a quick reference to the location of particular data fields. For example, line 28 identifies the symbols corresponding to the numbers in line 1.

```
 1 512 ØØ4 ØØ1 -1Ø +2.ØØØ-Ø3 +1.ØØØ-Ø3
 2 +4.ØØØ+Ø4 -1.ØØØ+Ø7 +1.ØØØ+Ø1
 3 Ø51 +9.99Ø-Ø1 +3.5ØØ+1Ø +5.ØØØ-Ø1 +3.ØØØ+Ø1 +Ø.ØØØ+Ø2 +Ø.ØØØ+21
 4 +Ø.ØØØ+ØØ +Ø.ØØØ+Ø6 +Ø.ØØØ+ØØ
 5 462 +9.99Ø-Ø1 +3.5ØØ+1Ø +5.ØØØ-Ø1 +3.ØØØ+Ø1 +Ø.ØØØ+Ø5 +Ø.ØØØ+21
 6 +Ø.ØØØ+ØØ +Ø.ØØØ+Ø6 +Ø.ØØØ+ØØ
 7 512 +Ø.ØØØ-Ø1 +3.5ØØ+1Ø +5.ØØØ-Ø1 +2.ØØØ+Ø1 +Ø.ØØØ+ØØ +Ø.ØØØ+21
 8 +4.ØØØ+Ø4 +1.ØØØ+Ø7 +1.ØØØ+Ø1
 9 +2 +1.ØØØ-Ø1
1Ø +1.ØØØ-1Ø +1.ØØØ+ØØ
11 +1.ØØØ-Ø8 +1.ØØØ+ØØ
12 ØØØØØ +2.76Ø+2Ø +2.5ØØ+ØØ +Ø.ØØØ+ØØ
13 ØØØØØ +Ø.ØØØ+12 +Ø.ØØØ+ØØ +Ø.5ØØ+Ø5
14 ØØØØØ +Ø.ØØØ+ØØ +Ø.ØØØ+ØØ +Ø.ØØØ+ØØ +Ø.ØØØ+ØØ
15 ØØØ +Ø.ØØØ+ØØ +4.ØØØ-1Ø Ø41 1132110
16 ØØØØ ØØ43 ØØØØ ØØØØ
17 1Ø23 1Ø23 1Ø23 1Ø23 1Ø23 1Ø23 1Ø23
18 1Ø23 1Ø23 1Ø23 1Ø23 1Ø23
19 111111111111111 Ø3
2Ø ØØ2 Ø1
21 Ø5Ø Ø1
22 51Ø Ø1
23
24 NAME  BOX 026
25
26  **************************************************************************
27
28 NC NG NE NINJ XMAX DTMAX
29
3Ø ERGY(IE,1) J() TEMP()
31 ZG(IG) GT() FØ() ZØ() Q() VC() JL()
32 ERGY(IE,IG) J() TEMP()
33
34 NFLUX FLUXAMP
35 FLUXT(IFLUX) FLUXA(IE,IFLUX)
36
37 NIONS IDNSTY MOQ TEMPI
38 NPROTS PDNSTY TEMPP TEMPE
39 NGPROT GPROT(IG)
4Ø
41 NOS TSTART TEND NSNAP    KPXP KPXI KPXE KQX KEX KVXX KPRINT
42 KFLX KXT NXTM NXTF
43 KVC KJL KJS KPMI KPMO KPEO  (BY GRIDS)
44 KUC KUL KUMI KUMO KUEO      (BY GRIDS)
45 KUI KUP KUE KNE KUIS KUOS KUGS KUM KUFS KUCS KULS KUIO KUS KUNET KUERR  ND
46 DIAGCELL DIAGTYP
47
48 FOR NOS NOT EQUAL TO ZERO:   NTSPOS=TEND, AND NPPP=NSNAP.
49
5Ø SPECIAL CONTROLS:
51       KPRINT.GT.7 PRINTS OUT DETAILS FOR EVERY PARTICLE
52       KPRINT FROM Ø TO 9 DETERMINE START OF RANDOM NUMBER GENERATOR
53       KPXE.EQ.2 FOR MOMENTUM PER COUL.
54       KPXE.EQ.3 FOR MOMENTUM PER ELECTRON
55       KQX.EQ.2 SUPPRESSES GRID CHARGE PLOTTING
```

FIGURE 4

The data in line one describes broad issues in the setup. In line 1, 512 is the number of cells in the model, and this corresponds to the identification "NC" in line 28. The number of grids, NG, including the two end grids is given as 004 in line 1. The number, NE, of energy levels to be emitted in the beam from each grid is 001. NINJ in line 28 is the number of macroparticles to be emitted from each grid at each energy level during each time step. In line 1, this is given as -10. A number less than zero causes one macroparticle to be emitted every -NINJ time steps, and a number greater than zero causes NINJ particles to be emitted each time step. XMAX, with a value of +2.000-03, is the length of the model in meters. DTMAX is the maximum allowed size of the time steps in the calculation. This allows the user to set DT lower than the automatically calculated value which is based on calculation stability requirements.

Line 2 gives the data on the electron emission of the first, in this case the only, energy level from grid 1. Line 30 identifies the parameters. In line 2, +4.000+04 is the mean energy of the beam in volts. The current density is -1.000+07 A/m^2. The beam temperature is +1.000+01 ev. In line 30, the subscripts for ERGY point out that this line applies to the IE energy level and grid 1. All items in line 2 have the same subscripts. If this example had more than one energy level, additional lines like line 2 would be needed for the additional energy levels.

Line 3 is the data defining grid 2 and the circuit between grids 1 and 2. ZG(IG) is the cell number where the grid is located. GT(IG) is the transparency of the grid. This may have a value from 0 to 1, and it determines electron absorption as described above. F0, Z0, and 0 are the

circuit parameters as described above in connection with Fig. 3. VC is the initial voltage on the circuit capacitance, and it is indicated in Fig. 1. JL is the initial current through the circuit inductor.

Line 4 is essentially like line 2, except that it applies to other grids. The pattern of lines 3 and 4 is repeated in lines 5 and 6 for grid 3 and in lines 7 and 8 for grid 4.

Line 9 starts the definition of the flux functions. The corresponding names are indicated in line 34. NFLUX is the number of break-point times in the functions as indicated in Fig. 2. FLUXAMP is the scaling factor described above. Lines 10 and 11 give the time, FLUXT, and amplitude, FLUXA, of the flux functions. This is indicated in line 35. The first point in all flux functions is zero amplitude at zero time, so the point specified in line 10 indicates a ramp from zero to one in the first 10^{-10} seconds. Line 11 specifies that the level will remain at one until 10^{-8} seconds. If more than one energy level were specified in line 1, the flux functions for these additional energy levels would be included in lines 10 and 11. This is done by extending these lines one entry for each additional energy level. If more breakpoint times were used, the pattern of lines 10 and 11 would be continued to provide a line defining each breakpoint.

Lines 12, 13 and 14 specify initial protons, ions and electrons in the model. The meanings are indicated in lines 37, 38, and 39. In line 12, NIONS is the number of macroparticles to be used to represent the ions. IDNSTY is the number of ions per cubic meter to be distributed uniformly throughout the model. MOQ is the ratio of mass to charge for the ion relative to that of a proton. Thus, a deuteron has an MOQ of 2, and singularly ionized oxygen has an MOQ of 16. TEMPI is the initial ion temperature in electron-volts.

In line 13, NPROTS is the number of macroparticles to be used to represent protons that are uniformly distributed throughout the space. PDNSTY is the number of protons per cubic meter, and TEMPP is the initial proton temperature in electron-volts. TEMPE is the initial temperature of the electrons that are added to neutralize the space charge of the ions and protons. This temperature also applies to the electrons used to neutralize grid protons.

In line 14, NGPROT is approximately the number of macroparticles that will be used to represent grid protons. The exact number used may vary slightly from this input. The remaining items on line 10 are the numbers of protons per square meter to be initially available at each grid. The second entry is for Grid 1, the third entry for Grid 2, etc. These protons are given the temperature specified in line 9 for protons.

On line 15, the first four entries control the problem run conditions. The names of these entries are indicated in line 41. Two control modes are available, and the choice is controlled by NOS, the first entry in line 15. If NOS is zero, the problem will be controlled by simulated time. The simulation always starts at time zero. TSTART in line 11 specifies the simulated time at which the first edits or snapshots are to be generated. TEND specifies the time that the problem is to stop, and NSNAP specifies the number of edits to be made. Thus, for this illustration, control is in the time mode, the first edit is at zero time, the simulation ends at 4×10^{-10} seconds, and 41 edits will be made. These edits occur at equal intervals, and they may not precisely match the end of the run at 4×10^{-10} seconds.

In the second control mode, the first item in line 15 would be greater than zero. Then the problem will run for that number of time steps. The second entry in line 15 is still the time that output will start. The third item in line 15 is the number of time steps between edits, and the fourth item is the number of edits. This is the meaning of the note in line 48.

The last seven digits on line 15 control the generation of outputs. The first six of these control graphics. If the digit is zero, the corresponding plot will not be made. If the digit is not 0, the plot will be made. Some of these provide additional controls when the value is 1 to 9. The first six of these digits control plots of:

proton dot plots of momentum vs. position.
ion dot plots of momentum vs. position.
electron dot plots of momentum vs. position.
total charge vs. position.
electric field vs. position.
potential vs. position.

The seventh digit of the last group on line 15 controls the printout of individual particle details at each edit. If this digit is 7, 8 or 9, the position, momentum, charge, of every particle will be printed. This may be useful at times, but it can generate a very large file when many particles are being used. In addition, this digit controls the initialization of the random number generator that is used to convert temperature to momentum. These and other special controls are indicated in lines 50 through 55.

Line 16 controls the plotting of various data vs. time. The first item, KFLX, in line 16 controls the plotting of flux vs. time for each energy level. This entry is coded as a binary function so the number to be entered is $2^{(i-1)}$, where i assumes the values of the energy levels to be plotted. For example, if four energy levels were being used in a problem and KFLX had a value of 15, all flux functions would be plotted. The flux for energy levels 1, 2 and 4 would be plotted if this item had a value of 11. (This scheme is also used for coding by grid numbers in lines 17 and 18.) (KFLX is not implemented at present.) The second item in line 16, KXT, controls the plotting of position vs. time trajectories for selected electrons. If this entry is zero, no plot will be made. If this entry is greater than zero, it is the number of injected electrons in the interval between selection of electrons that are plotted. If this entry is a multiple of the numbers of grids or the number of particles injected per time step, or the number of energy levels, there will be a tendency to select particles of one class. This can result in rather peculiar trajectory plots. Consequently, it is a good idea to use a prime number in this entry. The last two entries in line 16, NXTM and NXTF, have no effect at present.

Lines 17 and 18 control the plotting of grid and circuit data. The variable names are indicated in lines 43 and 44. These controls use the binary coding described in the last paragraph. With all entries set to 1023, all plots are normally produced. In line 17, KVC, KJL, and KJS are the circuit voltages and currents associated with each grid. KPMI controls the plotting of kinetic power input from each grid. KPMO and KPEO are the kinetic and electrical power outputs from each grid. In line 18, KUC and KUL are the

capacitive and inductive energy stored. KUMI, KUMO, and KUEO are the kinetic input energy, the kinetic output energy, and the electrical output energy at each grid.

Line 19 provides control of the 15 plots of energy summation. These are identified in line 45. KUI and KUP control the plots of kinetic energy of ions and protons. KUE controls the plot of the stored electrical energy. KNE controls the plot of the the number of electron particles in the problem. KUIS, KUOS, KUGS, and KUM control the plots of summation of kinetic input, kinetic output, electrical output, and stored kinetic energy.

In line 19, the last entry, 03, is the number, ND, of diagnostic grids that are to be plotted. The cell number, DIAGCELL, is given in lines 20 through 22. These plots show the current components to the right and to the left passing through the centers of the specified cells. These diagnostic cells have no other effect on the model. The variable DIAGTYP has not been implemented, but it is intended to provide some selection of variables measured in the diagnostic cells.

Line 23 must remain blank. In line 24, NAME is 4 letter identification of the calculation. This will normally appear in the names of both the ASCII printout and the graphics output. It is convenient to use it as the name of the data deck. The printout will be named XNAME, and the graphics file will be FX105*NAME, where NAME is the identification from line 24 and * is a random letter. When a calculation is run, the graphics output is automatically sent on fiche to the box specified in line 24.

1.2.7. Running VULTURE

VULTURE contains several parameters so it can be conveniently adjusted in numbers of grids, energy levels, flux break-points, particles, etc. This optimizes the code for the problems of interest and improves interactive operation on OCTOPUS. Consequently, this author should be contacted for an appropriately dimensioned version of the code. Otherwise, running the code on the CDC 7600s is not exceptional. The normal input line is:

```
VULTURE i=NAME / t v
```

2. CODE VALIDATION

In the development of VULTURE a number of comparisons to theory are used to provide reasonable confidence that the calculations from VULTURE are valid. These tests fall into four general categories. Each is discussed, and the results of code validation calculations are presented. The tests that have been run do not represent all permutations of parameters that can be checked against basic theory or known experimental results. Instead, these tests have been selected to provide reasonable confidence within the parameter ranges where the code is expected to be used initially. Consequently, anyone using this code may wish to confirm the validation within the parameter region of use.

2.1. GENERALLY CONSISTENT OPERATION

There are a number of factors that have been monitored throughout the development of VULTURE to assure that the code operates in a consistent and reasonable manner. For the most part, these items are obvious, but they have sometimes been the first indication of a bug. They are certainly necessary to the proper functioning of the code.

The first of these issues is that the code should produce symmetrical results when two problems are set up as mirror images. That is, if in one problem a beam is emitted from a cathode modeled at the left end of the system the results should be the same as if the beam were emitted from the right end of the system in a second problem. Likewise, if equal beams are emitted from the two ends the behavior of a diode should be symmetrical about the center of the diode. An example of this form of symmetry will be shown below involving the expansion of a hot plasma that is initially located in the center of the diode. Early in the development of the code, several validation calculations were made involving diode and triode configurations to be assured that this kind of symmetry exists consistently under various conditions of ion, proton, and electron populations.

It is essential that devices such as diodes and triodes behave in a reasonable, consistent way. During the development of VULTURE this was a primary test of the results. Electron beams are properly absorbed when they pass through grids. Ions and protons pass freely through interior grids and are reflected off of the end grids of the system. In a sense, this is a matter of looking at the broader picture to see that the general operation is qualitatively correct. In contrast, other calculations provide detailed

numerical comparisons to theory which might possibly seem correct even if the general operation were flawed.

Within the code there are several internal checks. The results are printed for the user to cross check to provide assurance that the calculations remain internally consistent. The first of these is a fractional energy error that is provided graphically and printed at the end of each time edit. This error is

$$\varepsilon = (W_{INPUT}-W_{OUTPUT}-W_{STORED})/W_{STORED}.$$

If this fractional error is less than 10^{-5} it is difficult to distinguish in the graphical output, but it can be read in the printed edit. When the energy stored remains high, these fractional errors usually do not exceed 10^{-2}, although some plasma simulations where the number of macroparticles is small will result in larger fractional errors. A larger fractional error does not necessarily mean a poor calculation. If the stored energy becomes small compared to the total input and output, this function may show a larger error even though the calculation is essentially correct. However, a small fractional error is a good indication. A quick glance at the fractional error curve on the graphical output usually gives adequate assurance.

The electric field, which results from the summation of charge from the left end of the system to the right end, should return to approximately zero. This appears in both the last field printed on the output edit and the last point on the graphical representation. There is nothing in the code to force this field to return to zero except the self consistency of the

calculations. Typically, this electric field will be 6 to 10 orders of magnitude below the peak fields in the main part of a diode.

The potential of the right end grid should equal the sum of the circuit voltages. These numbers appear at the end of each printed output edit. The summation of the potential from the field equations is the last number in the potential column for each time edit. The voltages of circuits are printed several lines below that on the output edit. The sum of the grid circuit voltages and the end grid potential should agree, or any error should be small compared to the maximum potential in the system. There is no internal check or forcing of either of these numbers except the internal consistency of the calculations. This is one of the more sensitive tests for internal consistency.

Plasma cutoff conditions and Debye length limitations are printed in the output edit.[5] These appear immediately after the literal reproduction of the input deck. Three numbers are presented for each source of potentially high density electrons. These sources are identified by printing the grid number and energy number. Energy number zero identifies the effects of electrons that are used to neutralize initial protons and ions. Those that are identified by a grid number zero are due to the electrons that are used to neutralize protons and ions that are initially distributed throughout the space of the problem. Other grid numbers associated with energy number zero apply to the electrons used to neutralize initial protons at that grid. The remaining combinations of grid and energy numbers apply to the electron beams emitted by the corresponding energy number at that grid. In calculating the plasma conditions for these emitted beams, the flux function is assumed to

have a nominal value of unity before it is multiplied by the scaling factor FLUXAMP. The numbers that are printed for each of these electron sources are the Debye length divided by DX, (λ_D/DX), the plasma period divided by DT, (τ_p/DT), and the plasma cut off frequency, f_p. Here, f_p is $1/2\pi\tau_p$. These numbers are arranged so λ_D/DX and τ_p/DT are good when they are greater than unity. Large numbers here do not provide complete assurance that there will be no problems in the calculations, but this does provide an indication or a flag that the user of the code should monitor. The actual plasma conditions should be checked more carefully if these numbers approach unity. The plasma frequency also serves as only a flag and not as an absolute limit.

Within the areas of initial interest in using VULTURE, any limitation due to τ_p/DT appears to be essentially nonexistent. The operation of any device of interest is more likely to be limited by plasma cutoff than to be a problem due to τ_p/DT. This is primarily a result of the DT in the code being based on criteria that is more severe than plasma cutoff. When plasma cutoff is a limitation, the calculation of device operation with plasma cutoff should be correct when τ_p/DT is adequate. Limitations due to λ_D/DX are another matter. The user of the code should monitor these conditions fairly carefully, particularly if the electron density becomes high due to either space charge neutralizing effects of ions and protons or high energy virtual cathodes. An example of this limitation will be shown below among the validation runs involving plasma expansion.

2.2. SIMPLE DIODES

One of the most basic and obvious tests one is tempted to make is to calculate the operation of a simple Child-Langmuir diode. In practice that does not work out well with VULTURE because of the Debye length limitation. The Child-Langmuir theory assumes an infinite source of cold electrons at the cathode. In VULTURE this results in a very small λ_D/DX, and the resulting calculation is unsatisfactory. This limitation is easily overcome in VULTURE by providing an initial temperature for the electrons at the cathode. When the electrons are sufficiently warm the Debye length will be somewhat greater than DX and the calculation will proceed reasonably. However, since the electrons leave the cathode with an initial energy the resulting current density across the diode will be somewhat greater than that predicted by the Child-Langmuir equation alone. Quate presents a derivation of a first order correction for this effect of a source of hot electrons.[6] The resulting current density is

$$J = 2.33\times10^{-6} \left(\phi^{3/2}/d^2\right)\left(1 + 2.69(\theta/\phi)^{1/2}\right) \quad , \tag{1}$$

where θ is the electron temperature in electron volts. In this formula the voltage, θ, and distance, d, have slightly different meanings than the actual applied voltage and anode to cathode spacing in the usual Child-Langmuir problem. To illustrate the meaning of these two quantities, Fig. 5 shows the potential distribution resulting from a VULTURE calculation of a one centimeter diode. In this calculation, electrons with a 1500 ev temperature are emitted from the right end plate which is biased at -50 kV. The resulting

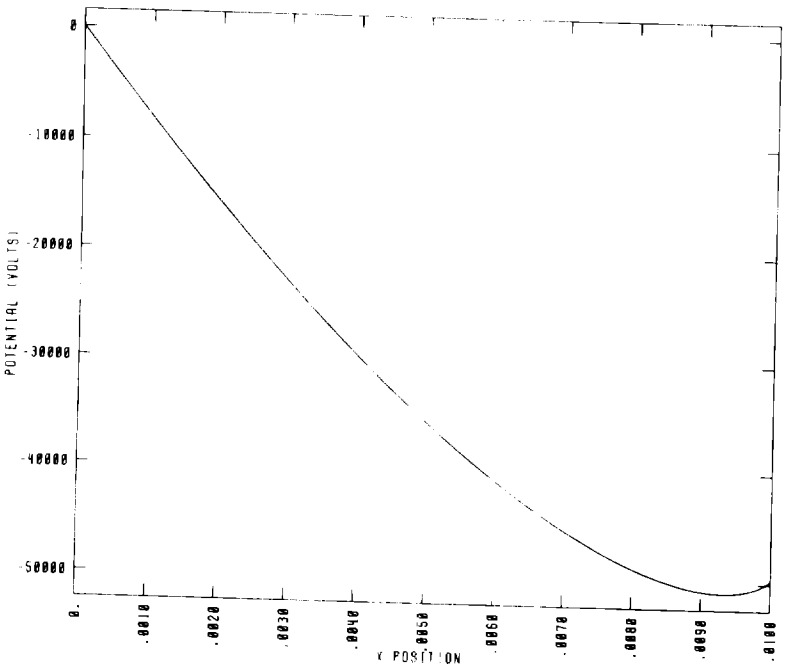

Figure 5

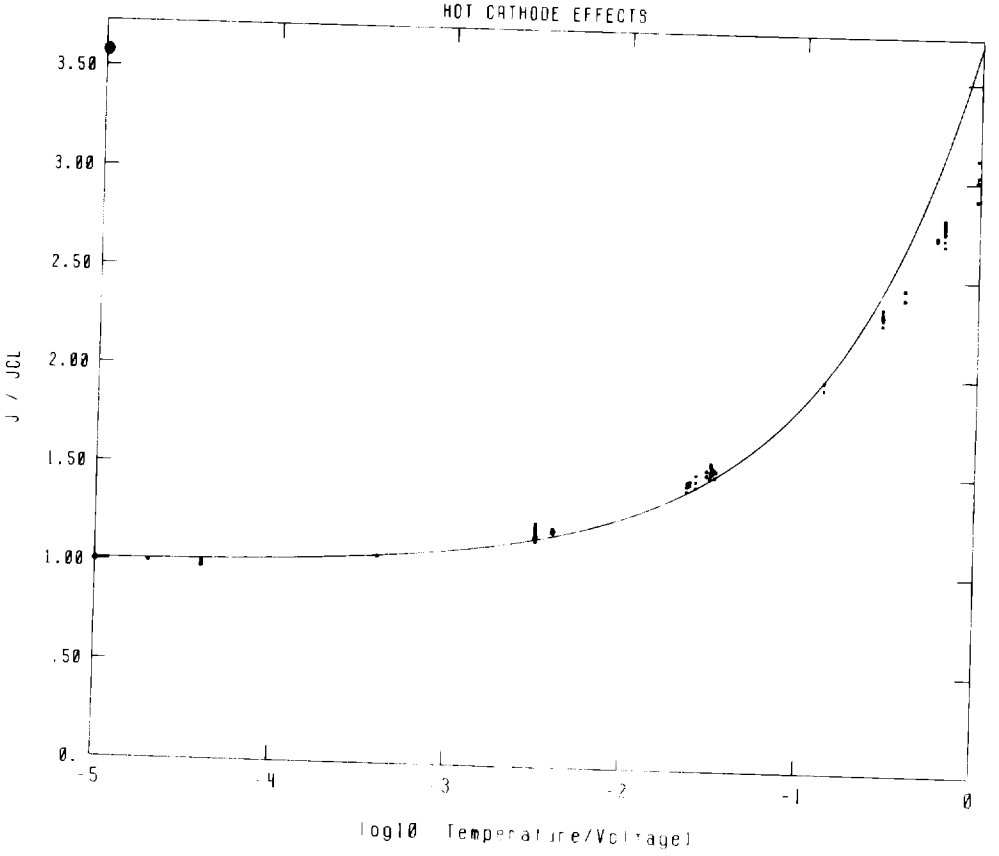

Figure 6

potential distribution has a minimum of -50.94 kV at 0.9335 cm. This distance and potential are the appropriate numbers to use in Equation 1. With this interpretation it is convenient to normalize Equation 1 as

$$J/J_o = 1 + 2.69\ (\theta/\phi)^{1/2} \quad . \tag{2}$$

Equation 2 is the curve plotted in Fig. 6, and the data points resulting from several VULTURE calculations are compared. This involves an assortment of anode to cathode spacings, cathode electron temperatures, and diode bias voltages.

Part of the results from one of these calculations are shown in Fig. 7. In this case, the beam energy is 10^{-3} V, and the temperature is 1500 eV. The diode spacing is 0.01 m. The available beam current density is 1.3×10^6 A/m^2. The results shown in Fig. 7 are: (a) macroparticle momentum vs. position after the steady state operation is established, (b) E field vs. position at the same time, (c) potential vs. position, (d) position vs. time trajectories for some particles, (e) the diode current density vs. time, and (f) the number of macroparticles vs. time. The current density and particle count show the steady state operation of the diode. The snapshots of momentum, field and potential are taken late in this time frame, at 0.954 ns.

The noise on the current density plot is reflected in the data points of in Fig. 6, where two to twelve data points are used from each diode calculation. The potential minimum, position, and current density for each of these data points is used in Equation 1 and plotted as a point in Fig. 6. This noise shown in Fig. 7e is the source of the spread of the data in Fig. 6.

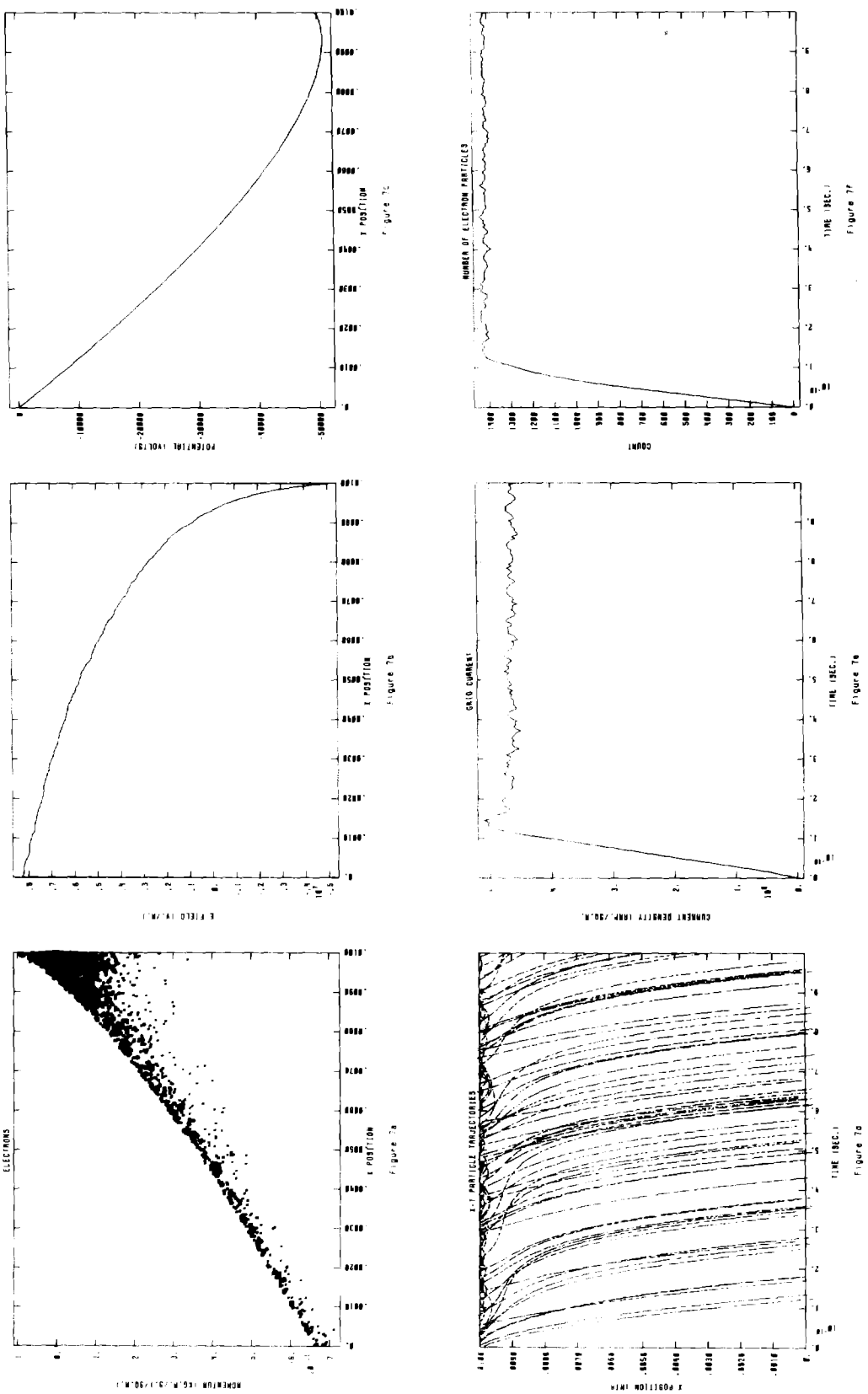
ELECTRONS
x POSITION
TIME (SEC.)
CURRENT DENSITY (AMP./SQ.M.)
GRID CURRENT
E FIELD (V/M)
POTENTIAL (VOLTS)
NUMBER OF ELECTRON PARTICLES
COUNT

Figure 7

The 1500 ev thermal spread of the beam clearly shows in Fig. 7a. The excess numbers of particles, as a result of the available current density being about five times the resulting space charge limited flow, show up in Figs. 7a and 7d. In Fig. 7a, this excess results in particles of positive momentum at the cathode. In Fig. 7d, the trajectories of some of these returning particles can be seen.

Figure 8 is essentially the same as Fig. 7, except that the temperature of the cathode electrons is only 20 eV. This results in a space charge limited beam current that is much closer to the Child-Langmuir limit. The lower thermal spread of the beam is most evident in Fig. 8a.

Generally, the results of these diode calculations, which are summarized in Fig. 6, agree quite well with theory. The slight deviation from theory at high temperature may result from limitations in VULTURE, but it may also result form limitations of this first order correction for temperature presented by Ouate. Refinement of this theory and resolution of this issue remains to be done. However, this seems to be a minor point.

2.3. PLASMA DEVICES

A series of calculations has been made to show the operation of VULTURE in calculating dense plasmas. These calculations are for relatively simple plasma expansion problems that can be compared directly to theory developed by Jacques Denavit.[7] For these calculations the model is a diode initially containing a neutral plasma extending from 3/8 to 5/8 of the length of the diode. The ions are initially at zero temperature, and the electrons are given an initial temperature which has been varied over a number of runs. As

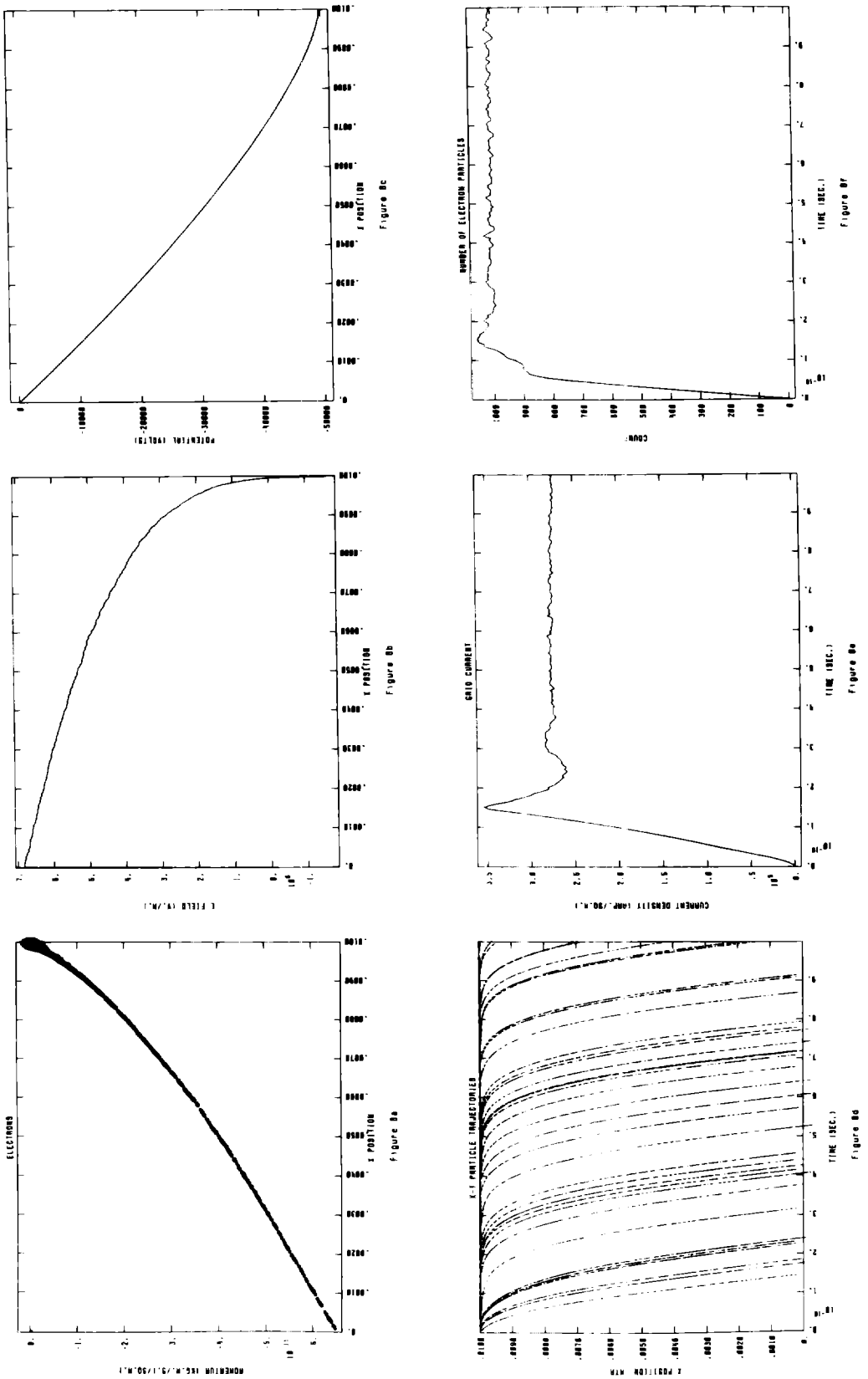
X-Y PARTICLE TRAJECTORIES
Z POSITION M
TIME (SEC.)
Figure 8d
CURRENT DENSITY (AMP./SQ.M.)
GRID CURRENT
TIME (SEC.)
Figure 8e
NUMBER OF ELECTRON PARTICLES
TIME (SEC.)
Figure 8f
ELECTRONS
X POSITION
Figure 8a
E FIELD (V./M.)
X POSITION
Figure 8b
POTENTIAL (VOLTS)
X POSITION
Figure 8c

Figure 8

the plasma expands, momentum and charge density distributions of the particles are observed and compared to theory. This relatively simple theory says that the ion momentum will increase in time and space as

$$P_i = (Z\, m_i \theta_e)^{1/2} + m_i\, x/t \quad , \tag{3}$$

and that the ion charge density will vary as

$$q_i = N_o Q_o \exp(-1-x(m_i/Z\theta_e)^{1/2}/t) \quad . \tag{4}$$

Here Z is the ion mass to charge ratio divided by that of a proton. θ_e is the electron temperature, m_i is the ion mass, N_o is the initial ion density, Q_o is the charge of a proton, x is position and t is time.

Typical results are shown in Fig. 9. Figure 9a shows ion macroparticle momentum vs. the position in the diode after 0.3 nanoseconds. The solid straight lines show the theoretical distribution represented by Equation 3. The momentum of each of approximately 3,000 of the particles is plotted. The total number of particles in this calculation was 25,000 ions and 25,000 electrons. Figure 9b shows the ion charge in each cell vs. position. This corresponds to the number of ions in each cell. The dashed lines show the theoretical exponential variation in charge density of Equation 4. Figure 9c shows the distribution of electron momentum verses position which is not theoretically predicted within this model. Again, approximately 3,000 particles of the 25,000 electrons are shown in the figure. Figure 9d shows the distribution of electron charge in the cells as a function of position.

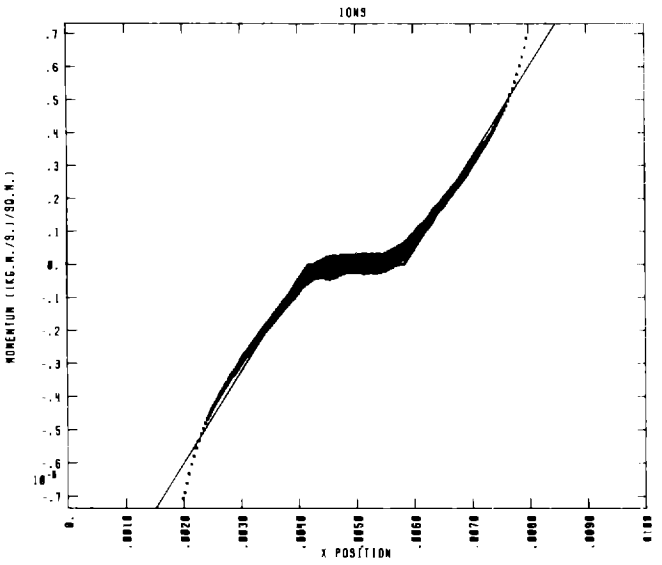

Figure 9a

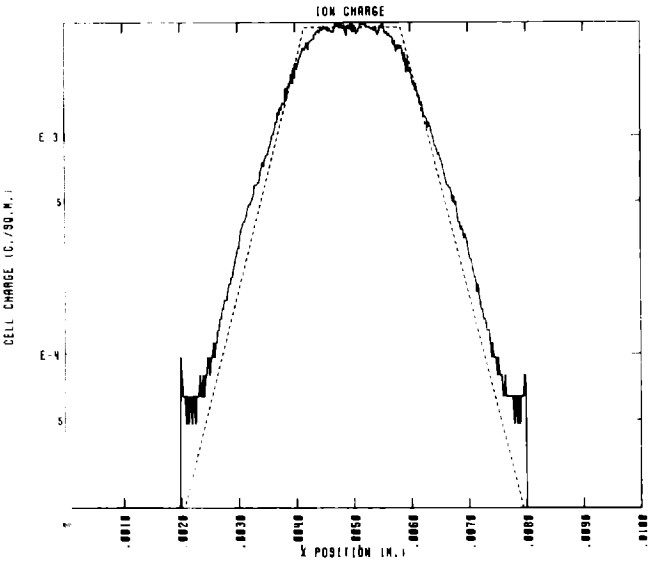

Figure 9b

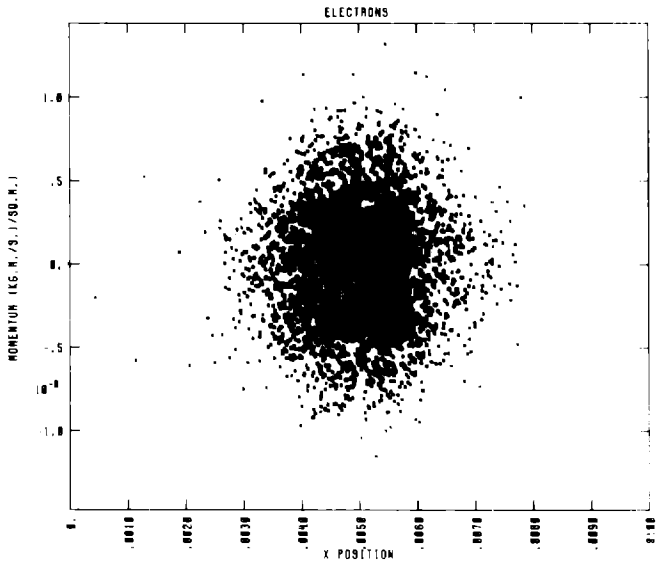

Figure 9c

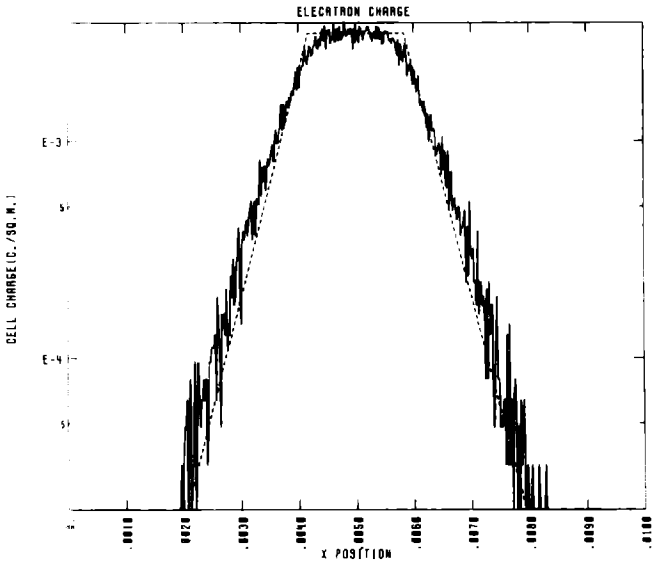

Figure 9d

Figure 9

This is also compared with the theoretical variation of Equation 4. For this calculation, the initial electron temperature was 10 keV and the initial ion density was 10^{21} ions per cubic meter. The resulting λ_D/DX was 2.4 and the resulting τ_p/DT was 17. The plasma cut off frequency was 142 GHz.

Figure 10 shows a similar diode expansion for different conditions. In this problem only 5,000 electrons and 5,000 ions were used, the initial ion density was 10^{23} ions per cubic meter, and the initial electron temperature was 100 keV. The resulting λ_D/DX is 0.76 and τ_p/DT is 1.7.

Figure 11 shows still another set of results. Again, 5,000 of each type of particle are being used. The initial ion density is 10^{23} ions per cubic meter and the electron temperature is 1 keV. The resulting λ_D/DX is 0.076 and the τ_p/DT is 1.7. This deviation from theory is the calculation error resulting from the Debye length becoming small compared to DX.

Several VULTURE problems have been run varying the ion density and electron temperature over a few orders of magnitude in the neighborhood of those presented in these three examples, and the results presented here are representative.

In making these systematic searches there was one other area where the code did not follow this simple theory. That is when the plasma density becomes low and the electron temperature becomes high. Under those conditions the theory ceases to be applicable because this theory is based on assumed plasma charge neutrality. That assumption is violated by the immediate escape of large numbers of high energy electrons.

In running the above calculations and examining variations of parameters, such as ion density and electron temperature, a systematic effort was being

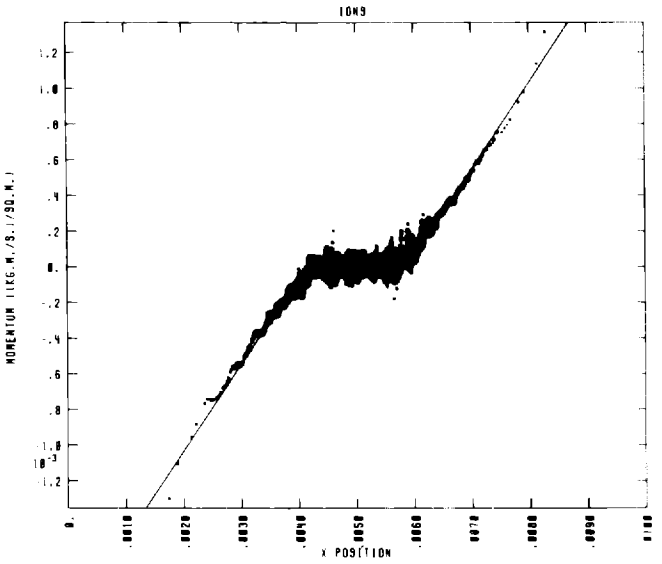

Figure 10a

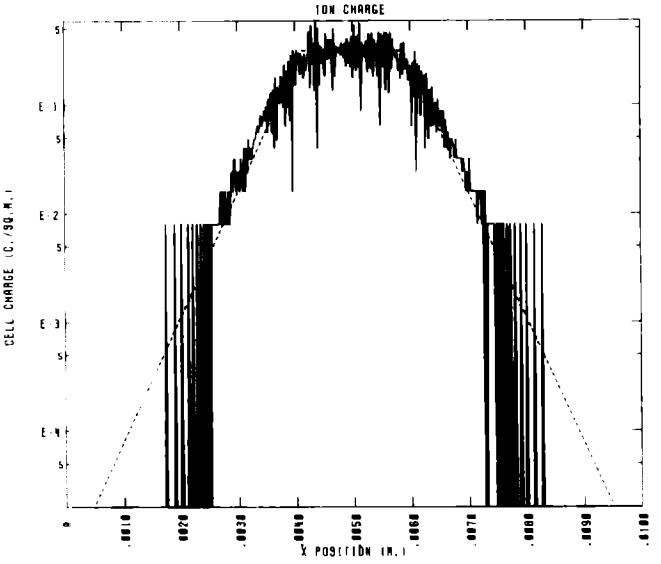

Figure 10b

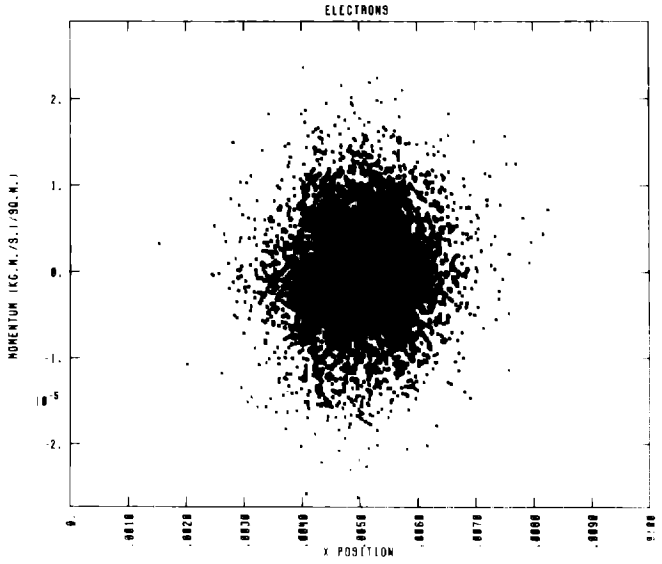

Figure 10c

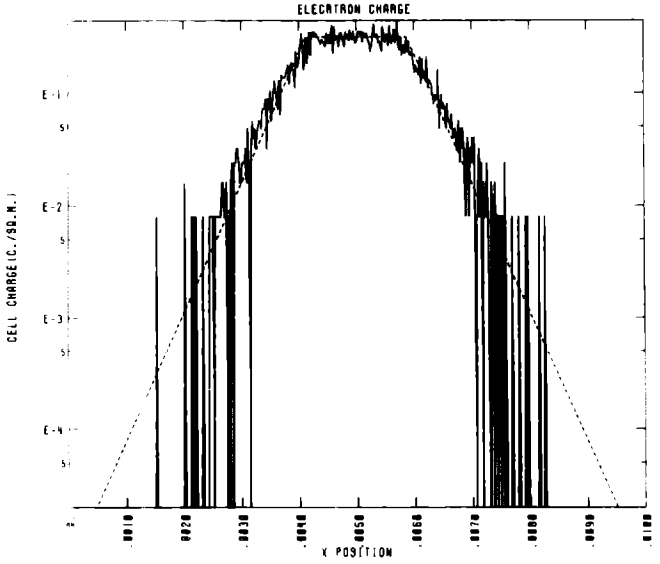

Figure 10d

Figure 10

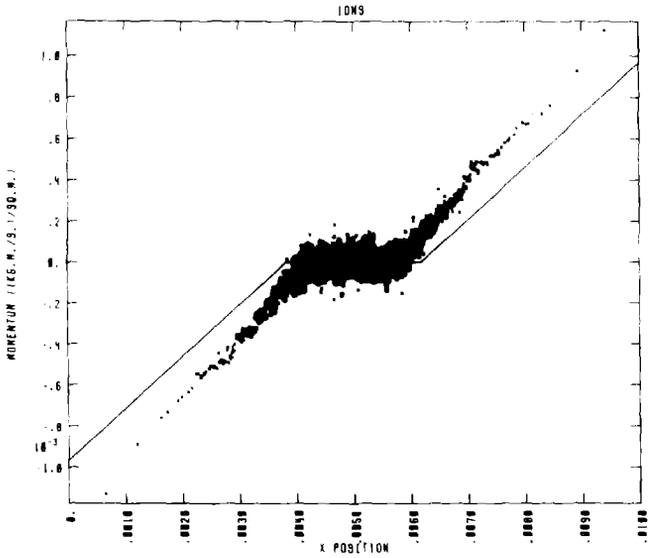

Figure 11a

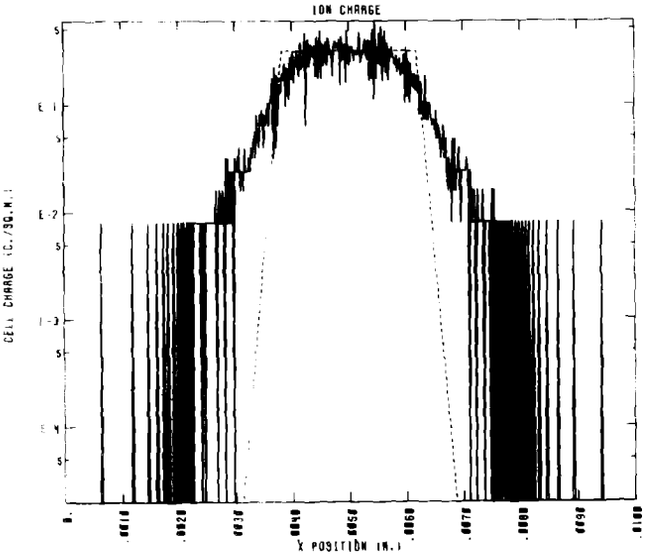

Figure 11b

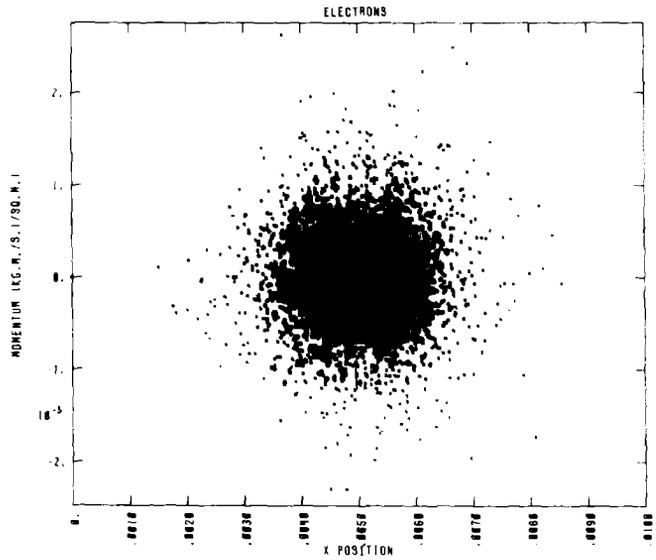

Figure 11c

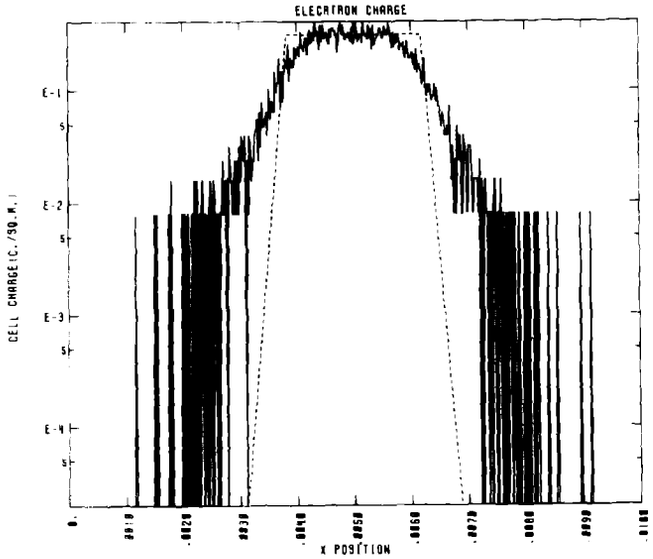

Figure 11d

Figure 11

made to understand the limits where the capability of VULTURE becomes questionable. The conclusion is that VULTURE is valid up to densities that produce the Debye length problem for the temperatures of interest. At the moment, that seems to be more capability then is needed by the code for the issues of immediate interest.

2.4. BIRDSALL AND BRIDGES DIODE

Birdsall and Bridges analyze and calculate the performance of diodes that are injected with monoenergetic electron beams.[8] In these diodes, a monoenergetic stream of electrons is injected into a diode region through a "cathode" or grid. The resulting behavior of the electrons is examined as a function of beam energy, V_0, normalized current density, α, and normalized frequency.

There are two major regions of operation that are separated by the value of $\alpha=8$. Here, α is defined as

$$\alpha = J_0/(2.33\times10^{-6}*V_0^{3/2}/d^2) \quad , \tag{5}$$

where J_0 is the injected current density in amperes per square meters and d is the diode spacing. For $\alpha<8$, the stream of electrons is stable. Birdsall and Bridges give an analytical prediction and computer simulations of the diode operation. One significant characteristic is the potential minimum that occurs between the plates of an externally shorted diode. Birdsall and Bridges results are compared to VULTURE calculations in Fig. 12. This shows the normalized potential minimum, $\phi=V/V0$, vs. α. The unlabeled curve is the

theoretical curve given by Birdsall and Bridges in their Equation 7, Chapter 3. Curve A is Birdsall and Bridges simulation results shown in their Fig. 3.10b. In Fig. 12, Curve B is VULTURE simulation results. In addition to this comparison, the results of VULTURE calculations showed the minimum potential at the diode center with symmetry about the center. This also agrees with the Birdsall and Bridges analysis and simulation.

For values of $\alpha>8$, the electron stream forms a virtual cathode, becomes unstable and oscillates. Birdsall and Bridges describe the general nature of this oscillation and give computer simulation results showing the frequency of oscillation, the variation in amplitude of the virtual cathode potential minimum, and the position of that minimum. Comparison of these results to VULTURE simulations are shown in Figs. 13, 14, and 15.

The comparison of normalized frequency vs. α is shown in Fig. 13. The base for normalizing frequency is the frequency having a period equal to the time required for an electron to cross the diode in the absence of space charge. Thus, the beam energy, V_0, enters into the frequency. In Fig. 13, Curve A is the result of Birdsall and Bridges simulation as given in their Fig. 3.11g. Curve B is the result of VULTURE simulation. The unlabled line shows a useful approximation to this frequency vs. α relationship:

$$f_n = 0.0555\ \alpha^{0.85} \quad . \tag{6}$$

The comparisons of normalized potential are shown in Fig. 14. For Birdsall and Bridges simulations, Curves A and B give the maximum and minimum values of the potential minimum for various values of α. Curves C and D give

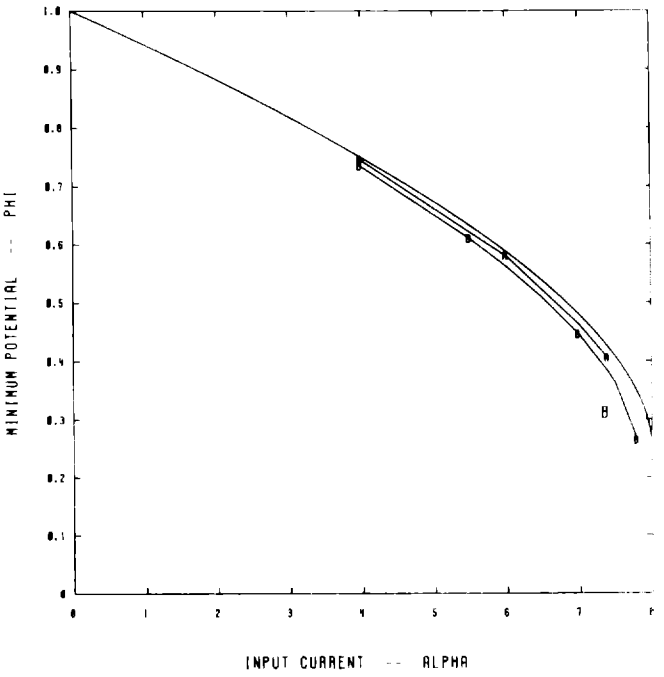

Figure 12

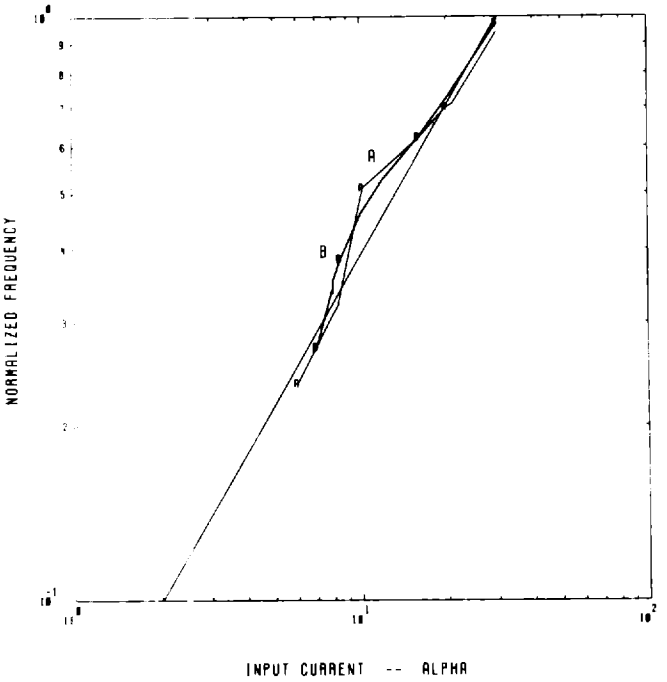

Figure 13

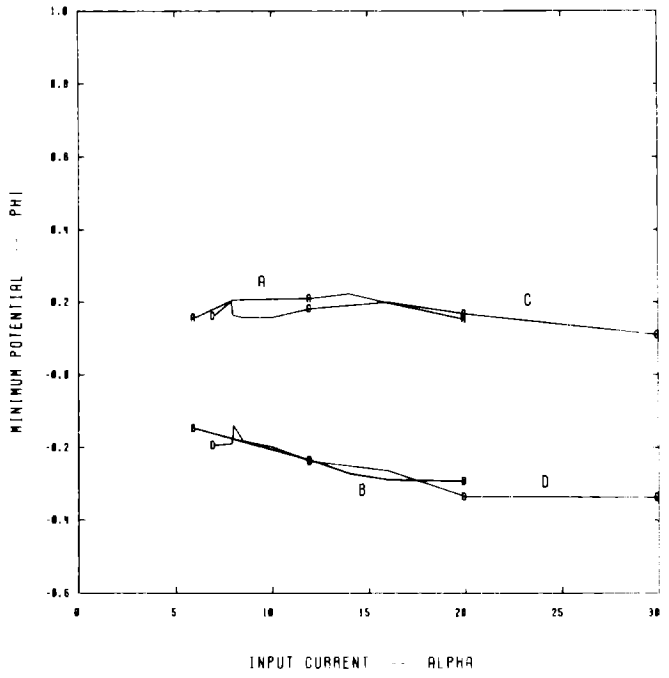

Figure 14

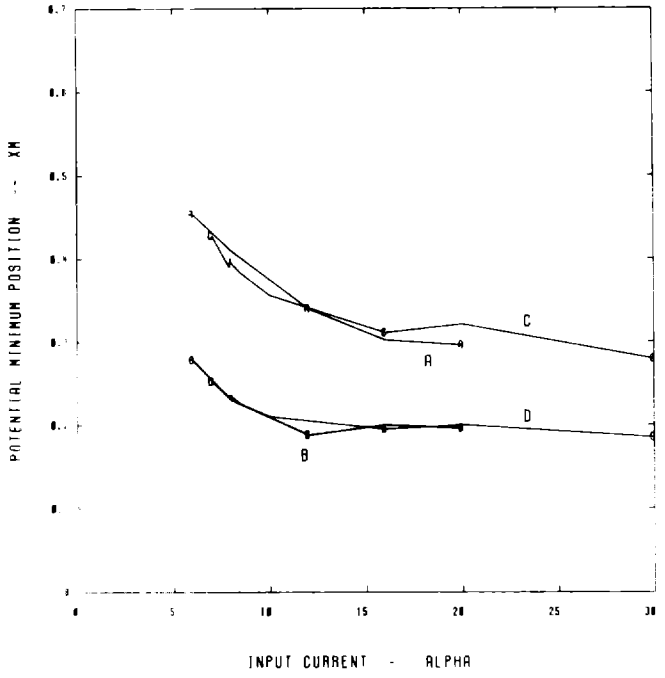

Figure 15

the corresponding maximum and minimum values for VULTURE simulations. The position of the potential minimum moves in the diode during oscillation. Comparison of this position vs. α is given in Fig. 15. This position of the minimum is the fraction of the diode spacing, d, measured from the emission cathode. Curves A and B give the results of Birdsall and Bridges simulations from their Figs. 3.11h. Curves C and D give the corresponding VULTURE results.

The most troublesome point that has been observed is a tendency of VULTURE simulations to oscillate at values of α slightly less than 8. This is shown by the limit of Curve B in Fig. 12. A similar effect shows up in Figs. 13, 14, and 15. When $\alpha>8$ is reduced to $\alpha<8$ during a calculation oscillations may continue. This is the source of the data points in these figures for $\alpha<8$. Under this condition, the Birdsall and Bridges simulations tend to show oscillations at lower values of α than VULTURE does. This combination of observations about the VULTURE simulations suggest that one should be cautious in interpreting results where the threshold of oscillation is an issue and $\alpha<8$.

The general conclusion of the comparisons of VULTURE to the cited Birdsall and Bridges work is that the agreement is very good. After having done this comparison, it seems that a more refined evaluation of the observed differences should include other sources of data.

ACKNOWLEDGMENT

In the development of VULTURE, there were many significant contributions by several people. Each of these is very much appreciated. I particularly thank Jacques Denavit for his discussions and guidance in both plasma physics and modeling issues.

REFERENCES

1. Birdsall, C. K. and Langdon, W. L., Plasma Physics via Computer Simulation, McGraw-Hill, 1984.

2. Denavit, J. and Kruer, W. L., How to Get Started in Particle Simulation, Comments Plasma Phy. and Controlled Fusion, Vol. 6, No. 1.

3. Rousset, S., Memo UCB/ERL M83/39.

4. Lawson, W. S., Memo UCB/ERL M84/37.

5. Craig, G. and Denavit, J., The Photoelectron Diode (Part I), LLNL memo, November 10, 1982.

6. Quate, C. F., "Shot Noise From Thermonic Cathodes," from Sumllin, L. D. and Haus, H. A., Noise in Electron Devices, John Wiley & Sons, 1959.

7. Denavit, J., Collisionless plaxma expansion into a vacuum, Phys. Fluids 22(7), July 1979.

8. Birdsall, C. K. and Bridges, W. B., Electron Dynamics of Diode Regions, Academic Press, 1966.